Confinement Effects and Acid Strength in Zeolites

Emanuele Grifoni
ETH Zurich https://orcid.org/0000-0002-3638-4929

GiovanniMaria Piccini
Institute of Computational Science, Università della Svizzera italiana (USI) https://orcid.org/0000-0002-3511-4281

Johannes Lercher
Technical University Munich

Vassiliki-Alexandra Glezakou (vanda.glezakou@pnnl.gov)
Pacific Northwest National Laboratory https://orcid.org/0000-0001-6028-7021

Roger Rousseau (roger.rousseau@pnnl.gov)
PNNL

Michele Parrinello (parrinello@phys.chem.ethz.ch)
Swiss Federal Institute of Technology in Zurich https://orcid.org/0000-0001-6550-3272

Article

Keywords: confinement effects, acid strength, zeolites, Brønsted acid sites (BAS)

Posted Date: September 23rd, 2020

DOI: https://doi.org/10.21203/rs.3.rs-79664/v1

Version of Record: A version of this preprint was published at Nature Communications on May 11th, 2021. See the published version at https://doi.org/10.1038/s41467-021-22936-0.

Abstract

Chemical reactivity and sorption in zeolites is coupled to confinement and - to a lesser extent- to the acid strength of Brønsted acid sites (BAS). In presence of water the zeolite Brønsted acid sites eventually convert into hydronium ions. The gradual transition from zeolite Brønsted acid sites to hydronium ions conversion in zeolites of varying pore size is examined by ab initio molecular dynamics combined with enhanced sampling based on well-tempered metadynamics and a recently developed set of collective variables. While at low water content (1-2 water/BAS) the acidic protons prefer to be shared between zeolites and water, higher water contents (n>2) invariably lead to solvation of the protons within a localized water cluster adjacent to the BAS. At low water loadings the standard free energy of the formed complexes is dominated by enthalpy and is associated with the acid strength of the BAS and the space around the site. Conversely, the entropy increases linearly with the concentration of waters in the pores, favors proton solvation and is independent of the pore size/shape.

Background

Brønsted acid catalysis is one of the most important classes of chemical conversion[1–11] and is critical for the reactions in petroleum refining and petrochemical industry, including for example hydrocarbon cracking[12–16], alkylation[17] and oligomerization, dehydration of alcohols [18–22], aldol condensation[23–25], ketonization[26], and esterification[27,28]. A wide variety of solid acids are used for such reactions with zeolites being one of the dominating groups [5,29,30].

Zeolites are tectosilicates with an impressive number of potential ways to link the corner shared SiO_4 tetrahedra forming a wide variety of pores and cavities[31–33]. Some of these framework tetrahedra are synthetically exchanged for other elements than Si^{4+}, typically Al^{3+}, but also Ga^{3+}, B^{3+}, Ge^{4+}, and Ti^{4+}. A charge imbalance is created, if the metal cation has a 3+ oxidation state. The resulting negative charge of -1 in the tetrahedron with oxygens is balanced by metal cations or H^+. The proton is stabilized as an OH group on one of the four oxygen atoms linking the tetrahedron to a neighboring one. It may fluctuate its position among the four oxygen atoms. This results in a “bridging” OH group with the potential to act as a Brønsted acid site (BAS) (**Figure 1**).

In its water free state, the ability of a BAS to protonate a base has been studied experimentally and theoretically to an impressive extent[6,34,35]. While early studies had suggested that zeolites would act as super acids[36] and show widely varying acid strength, it was found that the pK_A was lower than that of super acids and depended moderately on the crystal structure. Modern experiment and theory have shown conclusively that zeolites possess a high acid strength, but are relatively insensitive to structural effects and are mildly sensitive to the chemical composition[8,37]. It has been shown, however, that the constraints of the pores stabilize transition states of reacting molecules in a way that these materials show higher catalytic rates compared to counterparts of equal chemical composition on flat or mesoporous surfaces[7,38,39].

Aluminum containing zeolites have been shown to be hydrophilic. Purely siliceous materials are highly hydrophobic, i.e., they do not stabilize the continuous sorption of water molecules in a density equivalent or approaching liquid H_2O, even if engulfed in water[40–42]. The fact that it takes substantial external pressures to force water into zeolite pores of siliceous materials demonstrates that the loss of entropy from bulk to confined water prevents the full utilization of the whole pore volume[43].

Recently, it was shown that sorbed water molecules form clusters around the BAS, forming eventually hydrated hydronium ions, whose size is limited by the difference between the standard free energy of the water cluster in the pores compared to the aqueous phase[44,45]. For MFI zeolites with pores ~ 0.6 nm, this balancing act leads to hydrated hydronium clusters containing approximately eight water molecules.

The catalytic activity of such hydronium ions also benefits from the constrained environment, with rates approximately 1-2 orders of magnitude higher than those in an open aqueous environment [46–48]. Organic molecules appeared to adsorb in such environments only in the void left by hydrated hydronium ion clusters. This leads to marked discontinuities in the arrangements of molecules that have been shown to be equivalent to the impact of liquids of high ionic strength[44].

Understanding and controlling the impact of water ordering in zeolite pores leads to a better understanding of the hydrophobicity and allows us to predict and model the elementary steps of acid catalyzed reactions in confined spaces. This understanding requires addressing questions related to: (i) the nature and thermodynamics of solvation of the BAS in the presence of increasing chemical potentials of water and (ii) the size of hydrated hydronium ion clusters.

In this work, we examine these questions by a combination of ab initio molecular dynamics (AIMD) and enhanced sampling based on the metadynamics formalisms for studying the rare events dynamics and evaluating the associated free energy landscapes. There have been several prior studies of water in zeolites at the classical molecule dynamics[49–52] (CMD) and AIMD[53–57] levels of theory. The latter studies, which account for both reactivity and diffusion, reveal a complex behavior of the protonation state as a function of the number of waters and the nature of the BAS ranging from sharing of the proton equally between water and a BAS, to complete solvation of the proton within water clusters. Recently, AIMD combined with IR and high-resolution solid-state NMR on H-ZSM5 zeolites, showed that the interaction between the proton and the water cluster formed becomes weaker with increasing water loading, but plateaus out at a maximum solvation of 7-8 water molecules per BAS[44,45]. A preliminary computational study performed with AIMD simulations and static DFT calculations supported these conclusions[58], and showed that the bond distance between the acid proton and the releasing framework oxygen is proportional to the water concentration. Here, we ask if this formation of water clusters for proton solvation is an attribute of the MFI structure or if it is a generic property of all zeolites and their cavities?

We focus on the role of confinement on the specific population of water clusters and assess the enthalpic and entropic contributions to the zeolite acid-base equilibrium. Due to the presence of energy barriers

separating different protonation states, a standard simulation cannot fully address these questions. In order to overcome these limitations, we performed metadynamics simulations[59–61] to assess the relative free energies of potential protonation sites. We adapted a set of generalized collective variables, which enabled us to assess the relative acid-base properties of multiple sites and allowed to compute relative pKa values[58]. We use this method to investigate the protonation state of several zeolites as a function of water content to probe changes in acid strength and to determine if general behaviors exist to guide our understanding of the surface chemistry of protons in zeolites.

The protonation state of the BAS was studied for four different zeolites[62] (MFI, CHA, FAU, and GIS) with pore diameters ranging from 0.5-1.5 nm[63] (**Figure *2***). In all cases the BAS-proton pair correlation function changed with increasing water content showing at low loadings the formation of a complex in which the proton is shared between the BAS and the solvating water molecules. At high loadings complete protolysis occurred. It was observed that full protolysis is reached with four water molecules and further addition of water does not alter the equilibrium. Moreover, we find that for zeolites with a low concentration of BAS, the water clusters occupy only a small portion of the cavity independent of the cavity shape or size. This makes the entropic component in the acid-base equilibrium insensitive to the type of framework, while the enthalpic contribution, after an initial sharp decay, remains constant at all hydration levels. Thus, the zeolite structure plays only a minor role and the protonation free energy exhibits an approximately universal behavior.

Results And Discussion

Structure of water clusters within the zeolite framework

In order to understand, how water molecules are arranged in pores, we calculated the water density around a BAS. The radii of the spheres centered on the aluminum atom holding 90% of these densities were taken as a rough estimate of the portion of volume explored by the clusters, shown in **Figure 3**. It is noted that water molecules never reach some regions of the cavities and the fractions of occupied volume was not affected by the framework type.

The radii of these spheres are nearly the same in every tested zeolite and the volume increases with the number of water molecules at the same rate for every system. This is caused by the first water molecule remaining close to the zeolite framework (avoiding excessive charge separation) and to the hydrogen bond network that keeps the water clusters compact and prevents waters to diffuse inside the entire cavity.

An indication that the framework does not affect the cluster behavior comes from the analysis of their shapes. We know that these small clusters in the gas phase tend to organize in structures with defined geometrical arrangements[64–66]. Among these geometries, more interesting are the structures whose vertices are defined by 4 or more water molecules. A volume and a surface can be computed for these

polyhedra and from these we can get an estimation of their sphericity according to the Wadell definition[67]:

$$\psi_p = \frac{\pi^{\frac{1}{3}}(6V_p)^{\frac{2}{3}}}{A_p}. \qquad (1)$$

This formula defines the sphericity, Ψ_p, of a generic polyhedron as the ratio between its volume $_{Vp}$ and its surface $A_{p.}$ Ψ_p can assume values between 0 and 1, where, by definition, the sphericity of the cluster is unity for a sphere, and decreases in solids with lower symmetry. We know from literature that 4, 6 and 8 water molecules in gas phase are arranged in a tetragonal, prismoid and cubic shape, respectively[65]. We also know the Ψ values for all these structures in their regular shape. The sphericities of these clusters inside the zeolites were calculated and compared with the values extracted from the relevant MD simulations in gas phase, as well from the respective regular three-dimensional geometries (see **Table 1**). Results show that clusters confined into the zeolite frameworks have values comparable with the gas-phase ones.

Table 1. Water clusters sphericity, ψ, into four different zeolite cavities, in gas phase (GP) and the regular (R) three-dimensional geometries.

	n_{H_2O}	ψ_R	ψ_{GP}	ψ_{CHA}	ψ_{MFI}	ψ_{FAU}	ψ_{GIS}
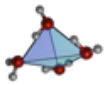	4	0.67	0.34	0.33	0.39	0.45	0.37
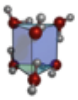	6	0.72	0.68	0.64	0.69	0.52	-
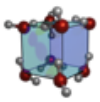	8	0.81	0.78	0.74	0.74	0.66	-

The analysis shows that water clusters confined in zeolite frameworks are not significantly impacted by a changing confinement. Previously, we reported a difference in shape and dynamic properties between a protonated octameric cluster and one confined within the channels of H-ZSMS5[44], which is in apparent contradiction to the current analysis. However, using a similar analysis to the current approach, we find that the previous trajectory, which is not as well sampled as the current one, can also be classified as having a similar volume as the gas phase counterpart.

From a statistical mechanics' point of view, entropy, and more precisely the translational contribution, is proportional to the accessible volume of the system. We also know that the positive charge can move

only inside the water network hopping from water to water through the hydrogen bond network. As a consequence, translational entropy grows proportionally to the volume of the water cluster and not necessarily with the zeolite cavity size. This implies that the entropic contribution to proton solvation is independent of the zeolite framework type and does not stem from the mobility of the overall cluster in the available pore.

Free energy surfaces for proton transfer.

In order to further probe this hypothesis, reaction free energies have been computed and decomposed to their enthalpic and entropic components. For this purpose, we adopted two recently developed descriptors[58], known as Collective Variables (CVs), as are a measure of the protonation state of our systems (s_p) and the distance between the charge carrier and the BAS site (s_d), see section S1 in SI for details. As can be seen from **Figure 5**, free energy surfaces (FESs) projected along the two CVs have roughly the same shape for all these systems with a deep and narrow minimum for and equal to zero and an elongated branch for equal to one. These states represent the undissociated and dissociated BAS, respectively.

In all four cases, we observe the same trends as a function of the number of waters. At low water loading (n = 1, 2) there is a preference for the proton to remain in the vicinity of the BAS site (s_p=0, s_d=0). However already at n=2 there is finite probability for the proton to move away from that wall by as much as 4 Å (s_p = 1, s_d = 4). This tendency increases with the number of water molecules, such that by n=8 the proton is completely solvated by water molecule (s_p = 1, s_d > 4). This is in agreement with previous AIMD studies which show that the proton becomes “solvated” at higher water concentrations, but remains close to the BAS site at low hydration levels[45].

From these FESs it is possible to distinguish three well defined thermodynamic states (**Figure 6**), i.e., an undissociated state with the proton covalently bonded to the zeolite (A), a state where the proton transfers to the closest water molecule forming a Zundel-like structure (B), and finally an end state where the hydronium ion is fully solvated and free to diffuse (C).

The FESs, thus, obtained were divided in these three different areas and integrated in order to get their relative population. From these populations, we can observe that the same trend of transferring the proton from the wall as a function of hydration level occurs in all four zeolites see **Figure 7**. In all cases, minimum A with the proton at the BAS becomes negligible once the water concentration exceeds 2 per BAS. It is minimum B, with the Zundel-like structure, where the most distinction between the zeolite frameworks occurs. Although the population of B is maximum at n=3 and drops off with increasing n, the rate at which it does so is not the same amongst the different zeolites. Its population decreases more rapidly the smaller the cage. Hence a more careful analysis of the energetics is required to quantitatively understand these trends.

The role of enthalpy and entropy in determining protonation state.

In order to understand the thermodynamic parameters determining the protonation state of water in zeolites, we use the relative trend in free energy between the undissociated (A) and the hydrolyzed states (B+C) as a function of the water loading. This function shows a universal behavior among different zeolites, see **Figure 8**. Most importantly, except for small differences, all systems present the same decay trend with increasing n, but are offset at n=1 due to the differing acid strength of the BAS as imposed by the zeolite framework. Indeed, shifting vertically all these curves by a constant value that compensate these small differences shows that all these curves can be collapsed in one. This implies that although the free energetics at low hydration level may depend on local structural features (small differences in enthalpy), the behavior at increasing n is being determined by a structurally insensitive free energy term.

To further probe this observation, we separate the free energy into contributions by the internal energy () and entropy ()[68] to determine the driving force for proton solvation. The trends in as a function of the number of waters are given in **Figure 9**, and shows that in all zeolites varies significantly between n=1-3, but tapers off to about 20 kJ mol^{-1} for n=3. This initial fast drop as well as the identical behavior of the four zeolites is attributed to the fact that the hydronium needs a certain number of water molecules to be stabilized, while the framework of the zeolites plays only a minor role. Once the cluster is sufficiently large, further addition of water molecules does not impact the solvation energy of the proton. The result clearly show that for more than 3 water molecules further association does not lead to a better enthalpic stabilization.

This is further substantiated when one considers the entropy computed (**Figure 9**), showing a nearly linear contribution to the free energy with increasing number of water molecules. All zeolites show a similar decrease with a slope of approximately -4.0 kJ mol^{-1}/H_2O molecule regardless of the cavity size, i.e., the entropy increases solely as a function of the number of waters, and is not influenced by the cavity size. Thus, we conclude that the main factor for this increase is related with the larger environment in which the proton can be mobile, i.e., the entropy of the proton depends on the size of the hydrogen bond network it is part of and that scales with the volume of the cluster. As the zeolite framework perturbs this property of the clusters very little this entropic stabilization of the proton is, to first order independent of the zeolite lattice.

Conclusions

The universal behavior of BAS solvation in a select group of zeolite frameworks was examined by means of ab initio metadynamics methods. Independent of cavity shape or size, water molecules cluster at BAS to fully solvate the proton at $n \geq 3$. The volume of the water cluster and entropy of solvation are independent of the zeolite cage structure. As a result, the free energetics of proton solvation follows a universal behavior in which the enthalpy contributes only very little to the stabilization of the cluster $n \geq 3$ and the entropic contribution grow linearly with the number of water molecules. This provides a straightforward extrapolation to predict the acid strength (pk_a) of a BAS in any Zeolite framework as a function of water content. The results show that water is not evenly distributed within the zeolite, but is

primarily located close to the negative charge in the zeolite lattice in order to minimize charge separation. Thus, overall the result set the computational framework necessary to model adsorption of organics and their reactivity in zeolites exposed to high chemical potentials of water.

Methods

Metadynamics Simulations: Breaking and forming covalent bonds, such of those involved in these reactions, implies high activation energies. Transitions between different protonation states occur on a time scale that can be reached with difficulty in a standard simulation. In order to accelerate the barrier crossings, metadynamics, an enhanced sampling method, is used to study chemical reactions. This method belongs to a class of enhanced sampling techniques based on the identification of the slow degrees of freedom involved in the reaction of interest[59,69,70]. These degrees of freedom, known in chemistry as Collective Variables, are functions of the atomic coordinates and must be chosen in order to extract the collective behavior connected to the reaction mechanism. Sampling is then accelerated by adding an external bias potential, a function of the chosen CVs, to the system potential energy. It is easy to understand how the choice of the CVs is crucial to obtain correct sampling.

In order to accelerate the exploration of every possible protonation state, as well as the diffusion of the hydronium ion inside the cavities, we adopted a recently developed set of CVs[58] extremely versatile for the study of reactions involving proton transfer. A first CV, , was used to enhance the exploration of new protonation states and push the zeolite to release a proton to the water cluster and vice versa. A second one, , was used to explore the distance between the BAS and the hydronium accelerating the diffusion of the charge carrier inside the cavity, see section S1 of SI for additional details. Born-Oppenheimer MD simulations were performed combined with Well-Tempered Metadynamics[59,60] using PLUMED2[71] driving the CP2K package[72]. The exchange-correlation energy, , was computed using PBE[73] functional, see below.

The four zeolites, with varying cavity shape and size shown in Figure 2, were studied loading each with an increasing number of water molecules per Brønsted acid site in a range from 1 to 8. The smallest zeolite tested, GIS-NaP1 could only accommodate up to 4 water molecules in its small cavity. The ratio Al:Si was kept constant at 1:95 which is comparable to typical experimental loadings.

AIMD Simulations: Periodic density functional theory (DFT) based AIMD were performed within the generalized gradient approximation (GGA) with the exchange correlation functional of Perdew, Burke and Ernzerhoff (PBE)[73] and Grimme's second-generation dispersion corrections (DFT-D2) as implemented in the CP2K package. Starting with the optimized zeolite unit cell with 95 SiO_2 units and a single Al atom for each system, AIMD simulations were performed with 1, 2, 3, 4 and 8 water molecule(s) at T=300K within the canonical *NVT* ensemble using a 0.5 fs time step and the CSVR[74] thermostat to determine the local structural properties. For each simulation, well-equilibrated trajectories of ~350 *ps* were collected to obtain reliable statistical properties. For further details of the simulations and system models see section S2 of the SI.

Declarations

Acknowledgements

E.G. GM. P. and M.P. thankfully acknowledge the financial support provided by the European Union Grant No. ERC-2014-AdG-670227/VARMET. V.-A.G., R.R. and J.A.L. were supported by the U.S. Department of Energy (DOE), Office of Science, Basic Energy Sciences, Chemical Sciences, Geosciences and Biosciences Division at Pacific Northwest National Laboratory (PNNL). E.G. was partially supported by the PNNL alternate sponsored fellowship program during a six month visit to the Richland campus. PNNL is operated by Battelle for the US Department of Energy under Contract DE-AC05-76RL01830. Computational resources were provided the Swiss National Supercomputing Centre (CSCS) under project IDs p503, s768 and s910 and the National Energy Research Scientific Computing Center (NERSC), a DOE Office of Science User Facility located at Lawrence Berkeley National Laboratory (LBNL) and operated under Contract No. DE-AC02-05CH11231.

References

(1) Taarning, E.; Osmundsen, C. M.; Yang, X.; Voss, B.; Andersen, S. I.; Christensen, C. H. Zeolite-Catalyzed Biomass Conversion to Fuels and Chemicals. *Energy and Environmental Science*. The Royal Society of Chemistry March 1, 2011, pp 793–804. https://doi.org/10.1039/c004518g.

(2) Climent, M. J.; Corma, A.; Iborra, S. Conversion of Biomass Platform Molecules into Fuel Additives and Liquid Hydrocarbon Fuels. *Green Chemistry*. Royal Society of Chemistry January 28, 2014, pp 516–547. https://doi.org/10.1039/c3gc41492b.

(3) Ravi, M.; Sushkevich, V. L.; Knorpp, A. J.; Newton, M. A.; Palagin, D.; Pinar, A. B.; Ranocchiari, M.; van Bokhoven, J. A. Misconceptions and Challenges in Methane-to-Methanol over Transition-Metal-Exchanged Zeolites. *Nature Catalysis*. Nature Publishing Group June 1, 2019, pp 485–494. https://doi.org/10.1038/s41929-019-0273-z.

(4) Jacobs, P. A.; Leuven, K. U. Acid Zeolites: An Attempt to Develop Unifying Concepts (P. H. Emmett Award Address, 1981). *Catal. Rev.* **1982**, *24* (3), 415–440. https://doi.org/10.1080/03602458208079659.

(5) Corma, A. Inorganic Solid Acids and Their Use in Acid-Catalyzed Hydrocarbon Reactions. *Chem. Rev.* **1995**, *95* (3), 559–614. https://doi.org/10.1021/cr00035a006.

(6) Gounder, R.; Iglesia, E. The Roles of Entropy and Enthalpy in Stabilizing Ion-Pairs at Transition States in Zeolite Acid Catalysis. *Acc. Chem. Res.* **2012**, *45* (2), 229–238. https://doi.org/10.1021/ar200138n.

(7) Gounder, R.; Iglesia, E. The Catalytic Diversity of Zeolites: Confinement and Solvation Effects within Voids of Molecular Dimensions. *Chem. Commun.* **2013**, *49* (34), 3491–3509. https://doi.org/10.1039/c3cc40731d.

(8) Jones, A. J.; Carr, R. T.; Zones, S. I.; Iglesia, E. Acid Strength and Solvation in Catalysis by MFI Zeolites and Effects of the Identity, Concentration and Location of Framework Heteroatoms. *J. Catal.* **2014**, *312*, 58–68. https://doi.org/10.1016/j.jcat.2014.01.007.

(9) Hemelsoet, K.; Van Der Mynsbrugge, J.; De Wispelaere, K.; Waroquier, M.; Van Speybroeck, V. Unraveling the Reaction Mechanisms Governing Methanol-to-Olefins Catalysis by Theory and Experiment. *ChemPhysChem*. June 3, 2013, pp 1526–1545. https://doi.org/10.1002/cphc.201201023.

(10) Göltl, F.; Michel, C.; Andrikopoulos, P. C.; Love, A. M.; Hafner, J.; Hermans, I.; Sautet, P. Computationally Exploring Confinement Effects in the Methane-to-Methanol Conversion over Iron-Oxo Centers in Zeolites. *ACS Catal.* **2016**, *6* (12), 8404–8409. https://doi.org/10.1021/acscatal.6b02640.

(11) Li, C.; Paris, C.; Martínez-Triguero, J.; Boronat, M.; Moliner, M.; Corma, A. Synthesis of Reaction-Adapted Zeolites as Methanol-to-Olefins Catalysts with Mimics of Reaction Intermediates as Organic Structure-Directing Agents. *Nat. Catal.* **2018**, *1* (7), 547–554. https://doi.org/10.1038/s41929-018-0104-7.

(12) Rahimi, N.; Karimzadeh, R. Catalytic Cracking of Hydrocarbons over Modified ZSM-5 Zeolites to Produce Light Olefins: A Review. *Applied Catalysis A: General*. Elsevier May 15, 2011, pp 1–17. https://doi.org/10.1016/j.apcata.2011.03.009.

(13) Haag, W. O. Catalysis by Zeolites – Science and Technology. *Stud. Surf. Sci. Catal.* **1994**, *84* (C), 1375–1394. https://doi.org/10.1016/S0167-2991(08)63680-0.

(14) Lercher, J. A.; van Santen, R. A.; Vinek, H. Carbonium Ion Formation in Zeolite Catalysis. *Catal. Letters* **1994**, *27* (1–2), 91–96. https://doi.org/10.1007/BF00806981.

(15) Xu, T.; Haw, J. F.; Munson, E. J. Toward a Systematic Chemistry of Organic Reactions in Zeolites: In Situ NMR Studies of Ketones. *J. Am. Chem. Soc.* **1994**, *116* (5), 1962–1972. https://doi.org/10.1021/ja00084a041.

(16) Corma, A.; Huber, G. W.; Sauvanaud, L.; O'Connor, P. Processing Biomass-Derived Oxygenates in the Oil Refinery: Catalytic Cracking (FCC) Reaction Pathways and Role of Catalyst. *J. Catal.* **2007**, *247* (2), 307–327. https://doi.org/10.1016/j.jcat.2007.01.023.

(17) Liu, Y.; Baráth, E.; Shi, H.; Hu, J.; Camaioni, D. M.; Lercher, J. A. Solvent-Determined Mechanistic Pathways in Zeolite-H-BEA-Catalysed Phenol Alkylation. *Nat. Catal.* **2018**, *1* (2), 141–147. https://doi.org/10.1038/s41929-017-0015-z.

(18) Cheung, P.; Bhan, A.; Sunley, G. J.; Iglesia, E. Selective Carbonylation of Dimethyl Ether to Methyl Acetate Catalyzed by Acidic Zeolites. *Angew. Chemie - Int. Ed.* **2006**, *45* (10), 1617–1620. https://doi.org/10.1002/anie.200503898.

(19) Jones, A. J.; Iglesia, E. Kinetic, Spectroscopic, and Theoretical Assessment of Associative and Dissociative Methanol Dehydration Routes in Zeolites. *Angew. Chemie - Int. Ed.* **2014**, *53* (45), 12177–

12181. https://doi.org/10.1002/anie.201406823.

(20) Chiang, H.; Bhan, A. Catalytic Consequences of Hydroxyl Group Location on the Rate and Mechanism of Parallel Dehydration Reactions of Ethanol over Acidic Zeolites. *J. Catal.* **2010**, *271* (2), 251–261. https://doi.org/10.1016/j.jcat.2010.01.021.

(21) Corma, A.; Huber, G. W.; Sauvanaud, L.; O'Connor, P. Biomass to Chemicals: Catalytic Conversion of Glycerol/Water Mixtures into Acrolein, Reaction Network. *J. Catal.* **2008**, *257* (1), 163–171. https://doi.org/10.1016/j.jcat.2008.04.016.

(22) Arora, S. S.; Nieskens, D. L. S.; Malek, A.; Bhan, A. Lifetime Improvement in Methanol-to-Olefins Catalysis over Chabazite Materials by High-Pressure H2 Co-Feeds. *Nat. Catal.* **2018**, *1* (9), 666–672. https://doi.org/10.1038/s41929-018-0125-2.

(23) Dumitriu, E.; Hulea, V.; Fechete, I.; Auroux, A.; Lacaze, J. F.; Guimon, C. The Aldol Condensation of Lower Aldehydes over MFI Zeolites with Different Acidic Properties. *Microporous Mesoporous Mater.* **2001**, *43* (3), 341–359. https://doi.org/10.1016/S1387-1811(01)00265-7.

(24) Kikhtyanin, O.; Kelbichová, V.; Vitvarová, D.; Kubů, M.; Kubička, D. Aldol Condensation of Furfural and Acetone on Zeolites. *Catal. Today* **2014**, *227*, 154–162. https://doi.org/10.1016/j.cattod.2013.10.059.

(25) Bui, L.; Luo, H.; Gunther, W. R.; Román-Leshkov, Y. Domino Reaction Catalyzed by Zeolites with Brønsted and Lewis Acid Sites for the Production of γ-Valerolactone from Furfural. *Angew. Chemie - Int. Ed.* **2013**, *52* (31), 8022–8025. https://doi.org/10.1002/anie.201302575.

(26) Pham, T. N.; Sooknoi, T.; Crossley, S. P.; Resasco, D. E. Ketonization of Carboxylic Acids: Mechanisms, Catalysts, and Implications for Biomass Conversion. *ACS Catalysis*. American Chemical Society November 1, 2013, pp 2456–2473. https://doi.org/10.1021/cs400501h.

(27) Corma, A.; Garcia, H.; Iborra, S.; Primo, J. Modified Faujasite Zeolites as Catalysts in Organic Reactions: Esterification of Carboxylic Acids in the Presence of HY Zeolites. *J. Catal.* **1989**, *120* (1), 78–87. https://doi.org/10.1016/0021-9517(89)90252-2.

(28) de la Iglesia, Ó.; Mallada, R.; Menéndez, M.; Coronas, J. Continuous Zeolite Membrane Reactor for Esterification of Ethanol and Acetic Acid. *Chem. Eng. J.* **2007**, *131* (1–3), 35–39. https://doi.org/10.1016/j.cej.2006.12.015.

(29) Corma, A. Solid Acid Catalysts. *Curr. Opin. Solid State Mater. Sci.* **1997**, *2* (1), 63–75. https://doi.org/10.1016/S1359-0286(97)80107-6.

(30) Primo, A.; Garcia, H. Zeolites as Catalysts in Oil Refining. *Chemical Society Reviews*. Royal Society of Chemistry November 21, 2014, pp 7548–7561. https://doi.org/10.1039/c3cs60394f.

(31) Ramdas, S.; Klinowski, J. A Simple Correlation between Isotropic 29Si-NMR Chemical Shifts and T-O-T Angles in Zeolite Frameworks. *Nature* **1984**, *308* (5959), 521–523. https://doi.org/10.1038/308521a0.

(32) Klinowski, J. Nuclear Magnetic Resonance Studies of Zeolites. *Progress in Nuclear Magnetic Resonance Spectroscopy*. Pergamon January 1, 1984, pp 237–309. https://doi.org/10.1016/0079-6565(84)80007-2.

(33) Rimer, J. D. Rational Design of Zeolite Catalysts. *Nature Catalysis*. Nature Publishing Group July 1, 2018, pp 488–489. https://doi.org/10.1038/s41929-018-0114-5.

(34) Li, G.; Pidko, E. A. The Nature and Catalytic Function of Cation Sites in Zeolites: A Computational Perspective. *ChemCatChem*. John Wiley & Sons, Ltd January 9, 2019, pp 134–156. https://doi.org/10.1002/cctc.201801493.

(35) Van Speybroeck, V.; Hemelsoet, K.; Joos, L.; Waroquier, M.; Bell, R. G.; Catlow, C. R. A. Advances in Theory and Their Application within the Field of Zeolite Chemistry. *Chemical Society Reviews*. 2015, pp 7044–7111. https://doi.org/10.1039/c5cs00029g.

(36) K. Tanabe; M. Misono; H. Hattori; Y. Ono. *New Solid Acids and Bases*, 1st ed.; Elsevier Science, 1990; Vol. 51.

(37) Boronat, M.; Corma, A. What Is Measured When Measuring Acidity in Zeolites with Probe Molecules? *ACS Catal.* **2019**, *9* (2), 1539–1548. https://doi.org/10.1021/acscatal.8b04317.

(38) Gounder, R.; Iglesia, E. Catalytic Consequences of Spatial Constraints and Acid Site Location for Monomolecular Alkane Activation on Zeolites. *J. Am. Chem. Soc.* **2009**, *131* (5), 1958–1971. https://doi.org/10.1021/ja808292c.

(39) Zicovich-Wilson, C. M.; Corma, A.; Viruela, P. Electronic Confinement of Molecules in Microscopic Pores. A New Concept Which Contributes to Explain the Catalytic Activity of Zeolites. *J. Phys. Chem.* **1994**, *98* (42), 10863–10870. https://doi.org/10.1021/j100093a030.

(40) Fasano, M.; Humplik, T.; Bevilacqua, A.; Tsapatsis, M.; Chiavazzo, E.; Wang, E. N.; Asinari, P. Interplay between Hydrophilicity and Surface Barriers on Water Transport in Zeolite Membranes. *Nat. Commun.* **2016**, *7* (1), 1–8. https://doi.org/10.1038/ncomms12762.

(41) Ohlin, L.; Berezovsky, V.; Öberg, S.; Farzaneh, A.; Holmgren, A.; Grahn, M. Effect of Water on the Adsorption of Methane and Carbon Dioxide in Zeolite Na-ZSM-5 Studied Using in Situ ATR-FTIR Spectroscopy. *J. Phys. Chem. C* **2016**, *120* (51), 29144–29152. https://doi.org/10.1021/acs.jpcc.6b09224.

(42) Zhou, T.; Bai, P.; Siepmann, J. I.; Clark, A. E. Deconstructing the Confinement Effect upon the Organization and Dynamics of Water in Hydrophobic Nanoporous Materials: Lessons Learned from

Zeolites. *J. Phys. Chem. C* **2017**, *121* (40), 22015–22024. https://doi.org/10.1021/acs.jpcc.7b04991.

(43) Humplik, T.; Raj, R.; Maroo, S. C.; Laoui, T.; Wang, E. N. Effect of Hydrophilic Defects on Water Transport in MFI Zeolites. *Langmuir* **2014**, *30* (22), 6446–6453. https://doi.org/10.1021/la500939t.

(44) Eckstein, S.; Hintermeier, P. H.; Zhao, R.; Baráth, E.; Shi, H.; Liu, Y.; Lercher, J. A. Influence of Hydronium Ions in Zeolites on Sorption. *Angew. Chemie - Int. Ed.* **2019**, *58* (11), 3450–3455. https://doi.org/10.1002/anie.201812184.

(45) Glezakou, V.-A. A.; Camaioni, D. M.; Lee, M. S.; Gutiérrez, O. Y.; Rousseau, R.; Wang, M.; Wan, C.; Jaegers, N. R.; Mei, D.; Wang, Y.; et al. Genesis and Stability of Hydronium Ions in Zeolite Channels. *J. Am. Chem. Soc.* **2019**, *141* (8), 12. https://doi.org/10.1021/jacs.8b07969.

(46) Liu, Y.; Vjunov, A.; Shi, H.; Eckstein, S.; Camaioni, D. M.; Mei, D.; Baráth, E.; Lercher, J. A. Enhancing the Catalytic Activity of Hydronium Ions through Constrained Environments. *Nat. Commun.* **2017**, *8* (1), 1–8. https://doi.org/10.1038/ncomms14113.

(47) Vjunov, A.; Hu, M. Y.; Feng, J.; Camaioni, D. M.; Mei, D.; Hu, J. Z.; Zhao, C.; Lercher, J. A. Following Solid-Acid-Catalyzed Reactions by MAS NMR Spectroscopy in Liquid Phase - Zeolite-Catalyzed Conversion of Cyclohexanol in Water. *Angew. Chemie - Int. Ed.* **2014**, *53* (2), 479–482. https://doi.org/10.1002/anie.201306673.

(48) Shi, H.; Eckstein, S.; Vjunov, A.; Camaioni, D. M.; Lercher, J. A. Tailoring Nanoscopic Confines to Maximize Catalytic Activity of Hydronium Ions. *Nat. Commun.* **2017**, *8* (1), 1–7. https://doi.org/10.1038/ncomms15442.

(49) Shirono, K.; Daiguji, H. Dipole Moments of Water Molecules Confined in Na-LSX Zeolites - Molecular Dynamics Simulations Including Polarization of Water. *Chem. Phys. Lett.* **2006**, *417* (1–3), 251–255. https://doi.org/10.1016/j.cplett.2005.09.130.

(50) Demontis, P.; Gulín-González, J.; Masia, M.; Suffritti, G. B. The Behaviour of Water Confined in Zeolites: Molecular Dynamics Simulations versus Experiment. *J. Phys. Condens. Matter* **2010**, *22* (28), 13. https://doi.org/10.1088/0953-8984/22/28/284106.

(51) Demontis, P.; Stara, G.; Suffritti, G. B. Behavior of Water in the Hydrophobic Zeolite Silicalite at Different Temperatures. A Molecular Dynamics Study. *J. Phys. Chem. B* **2003**, *107* (18), 4426–4436. https://doi.org/10.1021/jp0300849.

(52) Demontis, P.; Stara, G.; Suffritti, G. B. Molecular Dynamics Simulation of Anomalous Diffusion of One-Dimensional Water Molecule Chains in Li-ABW Zeolite. *Microporous Mesoporous Mater.* **2005**, *86* (1–3), 166–175. https://doi.org/10.1016/j.micromeso.2005.07.007.

(53) Bukowski, B. C.; Bates, J. S.; Gounder, R.; Greeley, J. Defect-Mediated Ordering of Condensed Water Structures in Microporous Zeolites. *Angew. Chemie - Int. Ed.* **2019**, *58* (46), 16422–16426.

https://doi.org/10.1002/anie.201908151.

(54) Schwarz, K.; Nusterer, E.; Blöchl, P. E. First-Principles Molecular Dynamics Study of Small Molecules in Zeolites. *Catal. Today* **1999**, *50* (3–4), 501–509. https://doi.org/10.1016/S0920-5861(98)00484-2.

(55) Vener, M. V.; Rozanska, X.; Sauer, J. Protonation of Water Clusters in the Cavities of Acidic Zeolites: (H 2O)N·H-Chabazite, n = 1-4. *Phys. Chem. Chem. Phys.* **2009**, *11* (11), 1702–1712. https://doi.org/10.1039/b817905k.

(56) Termath, V.; Haase, F.; Sauer, J.; Hutter, J.; Parrinello, M. Understanding the Nature of Water Bound to Solid Acid Surfaces. Ab Initio Simulation on HSAPO-34. *J. Am. Chem. Soc.* **1998**, *120* (33), 8512–8516. https://doi.org/10.1021/ja981549p.

(57) Coudert, F. X.; Cailliez, F.; Vuilleumier, R.; Fuchs, A. H.; Boutin, A. Water Nanodroplets Confined in Zeolite Pores. *Faraday Discuss.* **2008**, *141* (0), 377–398. https://doi.org/10.1039/b804992k.

(58) Grifoni, E.; Piccini, G.; Parrinello, M. Microscopic Description of Acid–Base Equilibrium. *PNAS* **2019**, 201819771. https://doi.org/10.1073/pnas.1819771116.

(59) Laio, A.; Parrinello, M. Escaping Free-Energy Minima. *Proc. Natl. Acad. Sci.* **2002**, *99*, 12562.

(60) Barducci, A.; Bussi, G.; Parrinello, M. Well-Tempered Metadynamics: A Smoothly Converging and Tunable Free-Energy Method. *Phys. Rev. Lett.* **2008**, *100* (2), 1–4. https://doi.org/10.1103/PhysRevLett.100.020603.

(61) Valsson, O.; Tiwary, P.; Parrinello, M. Enhancing Important Fluctuations: Rare Events and Metadynamics from a Conceptual Viewpoint. *Annu. Rev. Phys. Chem.* **2016**, *67* (1), 159–184. https://doi.org/10.1146/annurev-physchem-040215-112229.

(62) Baerlocher, C.; McCusker, L. B. Database of Zeolite Structures http://www.iza-structure.org/databases/ (accessed Jul 17, 2020). https://doi.org/http://www.iza-structure.org/databases/.

(63) Smith, J. V. Topochemistry of Zeolites and Related Materials. 1. Topology and Geometry. *Chem. Rev.* **1988**, *88* (1), 149–182. https://doi.org/10.1021/cr00083a008.

(64) Maheshwary, S.; Patel, N.; Sathyamurthy, N.; Kulkarni, A. D.; Gadre, S. R. Structure and Stability of Water Clusters (H 2 O) n , n = 8-20: An Ab Initio Investigation. *J. Phys. Chem. A* **2001**, *105* (46), 10525–10537. https://doi.org/10.1021/jp013141b.

(65) Gregory, J. K.; Clary, D. C. Structure of Water Clusters. The Contribution of Many-Body Forces, Monomer Relaxation, and Vibrational Zero-Point Energy. *Journal of Physical Chemistry*. 1996, pp 18014–18022. https://doi.org/10.1021/jp9616019.

(66) Laasonen, K.; Parrinello, M.; Car, R.; Lee, C.; Vanderbilt, D. Structures of Small Water Clusters Using Gradient-Corrected Density Functional Theory. *Chem. Phys. Lett.* **1993**, *207* (2–3), 208–213. https://doi.org/10.1016/0009-2614(93)87016-V.

(67) Wadell, H. Volume, Shape, and Roundness of Quartz Particles. *J. Geol.* **1935**, *43* (3), 250–280. https://doi.org/10.1086/624298.

(68) Gallet, G. A.; Pietrucci, F.; Andreoni, W. Bridging Static and Dynamical Descriptions of Chemical Reactions: An Ab Initio Study of CO 2 Interacting with Water Molecules. *J. Chem. Theory Comput.* **2012**, *8* (11), 4029–4039. https://doi.org/10.1021/ct300581n.

(69) Torrie, G. M.; Valleau, J. P. Nonphysical Sampling Distributions in Monte Carlo Free-Energy Estimation: Umbrella Sampling. *J. Comput. Phys.* **1977**, *23* (2), 187–199. https://doi.org/10.1016/0021-9991(77)90121-8.

(70) Valsson, O.; Parrinello, M. Variational Approach to Enhanced Sampling and Free Energy Calculations. *Phys. Rev. Lett.* **2014**, *113* (9), 1–5. https://doi.org/10.1103/PhysRevLett.113.090601.

(71) Tribello, G. A.; Bonomi, M.; Branduardi, D.; Camilloni, C.; Bussi, G. PLUMED 2: New Feathers for an Old Bird. *Comput. Phys. Commun.* **2014**, *185* (2), 604–613. https://doi.org/10.1016/j.cpc.2013.09.018.

(72) Vandevondele, J.; Krack, M.; Mohamed, F.; Parrinello, M.; Chassaing, T.; Hutter, J. Quickstep: Fast and Accurate Density Functional Calculations Using a Mixed Gaussian and Plane Waves Approach. *Comput. Phys. Commun.* **2005**, *167* (2), 103–128. https://doi.org/10.1016/j.cpc.2004.12.014.

(73) Perdew, J. P.; Burke, K.; Ernzerhof, M. Generalized Gradient Approximation Made Simple. *Phys. Rev. Lett.* **1996**, *77* (18), 3865–3868. https://doi.org/10.1103/PhysRevLett.77.3865.

(74) Bussi, G.; Donadio, D.; Parrinello, M. Canonical Sampling through Velocity Rescaling. *J. Chem. Phys.* **2007**, *126* (1). https://doi.org/10.1063/1.2408420.

Figures

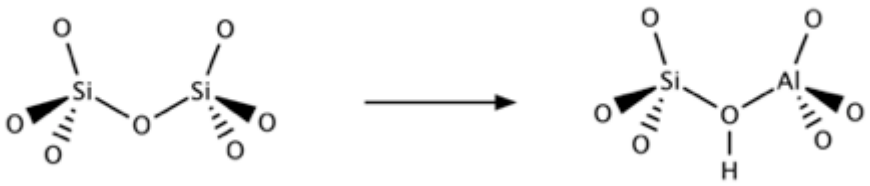

Figure 1

Brønsted Acid sites are formed when trivalent metals are substituted for Si4+ in the zeolite frame.

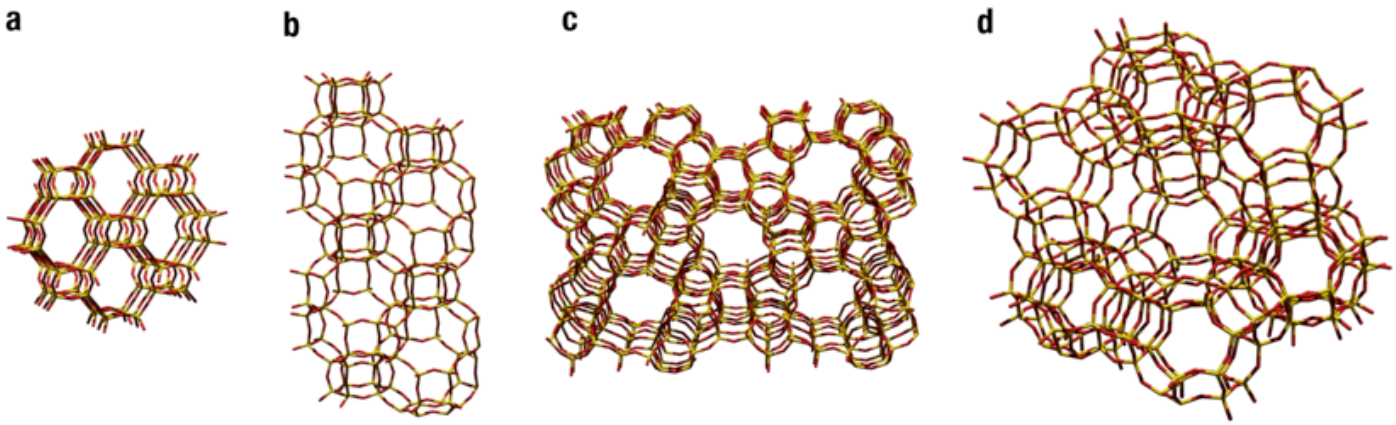

Figure 2

Structures of zeolites employed in this work. (a) GIS, which consists of 8 and 4 ring size cages with diameter 4.97 Å, (b) CHA which consists of 8, 6 and 4 ring size cages with diameter 7.37 Å, (c) MFI which consists of 10, 6, 5 and 4 ring size cages.

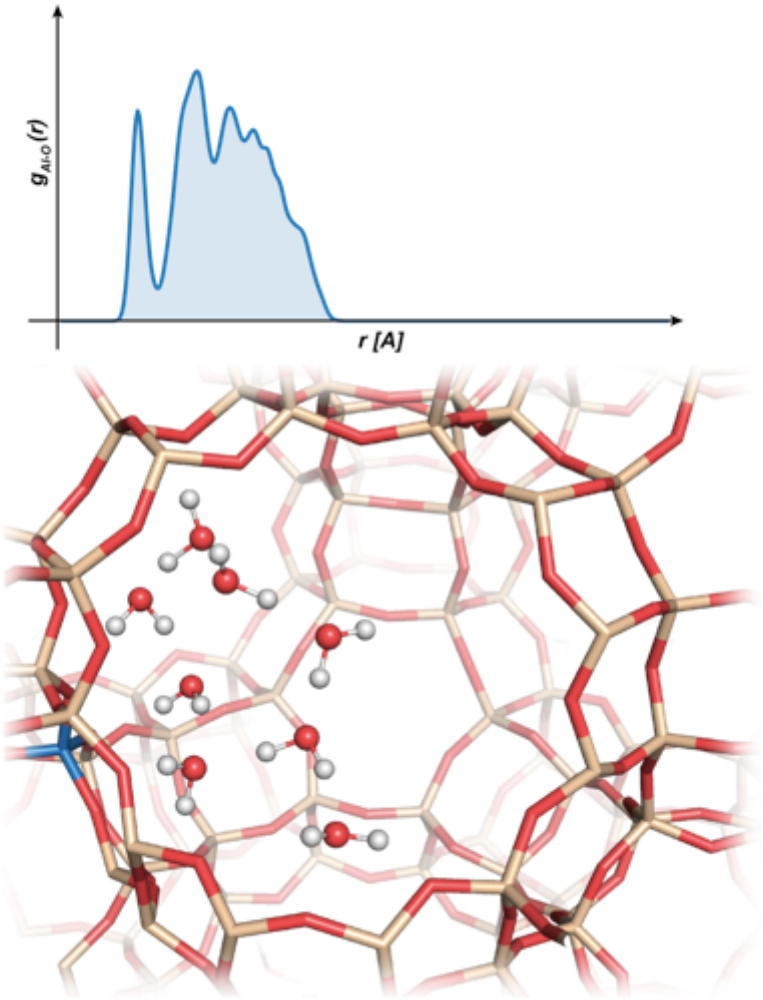

Figure 3

Al-Ow radial distribution function overlaid on a faujasite cavity and its water molecules

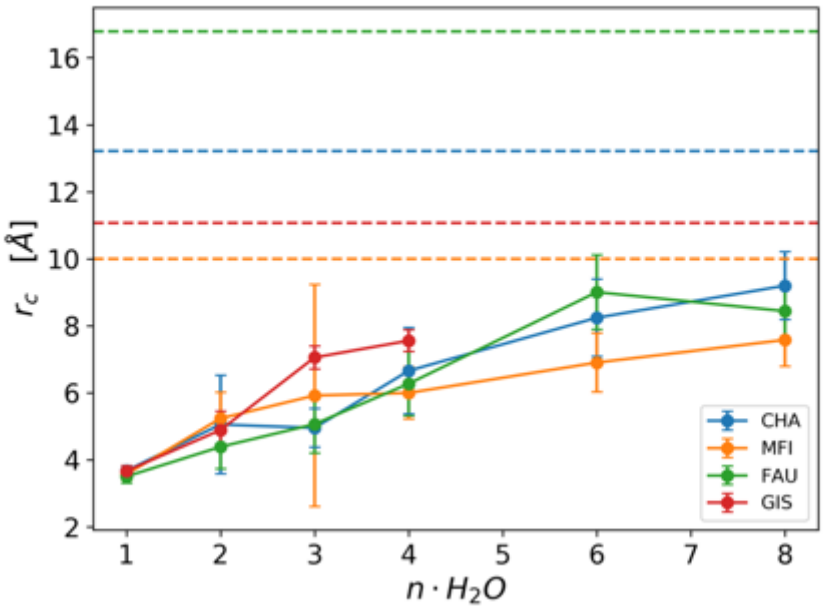

Figure 4

Radius of a sphere around the aluminum atom enclosing the 90% of the water density. Dashed lines report the maximum Al-Si distances in the respective cavities. The dashed lines indicate the diameters of the main channel or cavity.

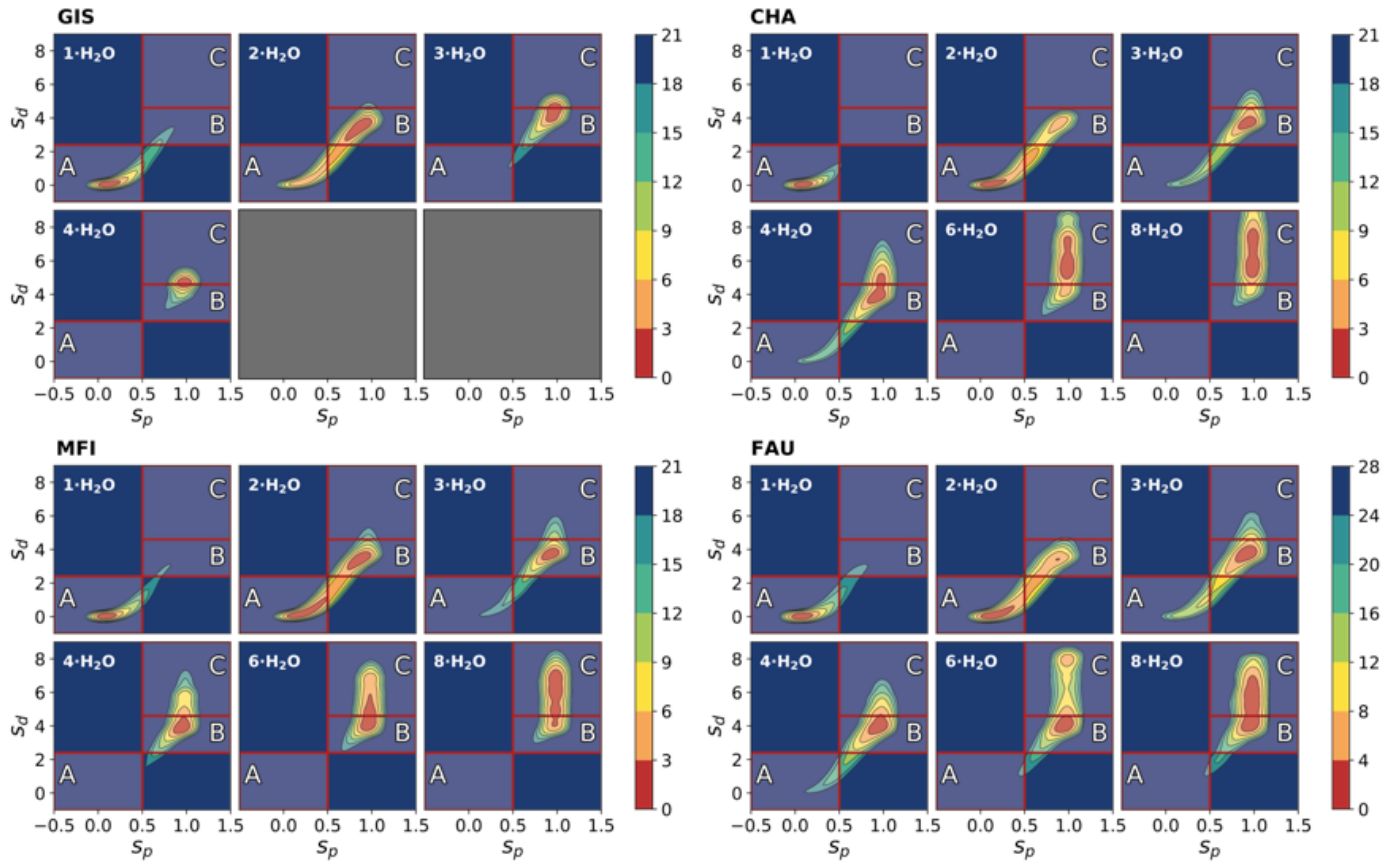

Figure 5

GIS, CHA, MFI and FAU free energy surfaces along sp and sd at different hydration levels. Differences in free energies are expressed in kJ mol-1.

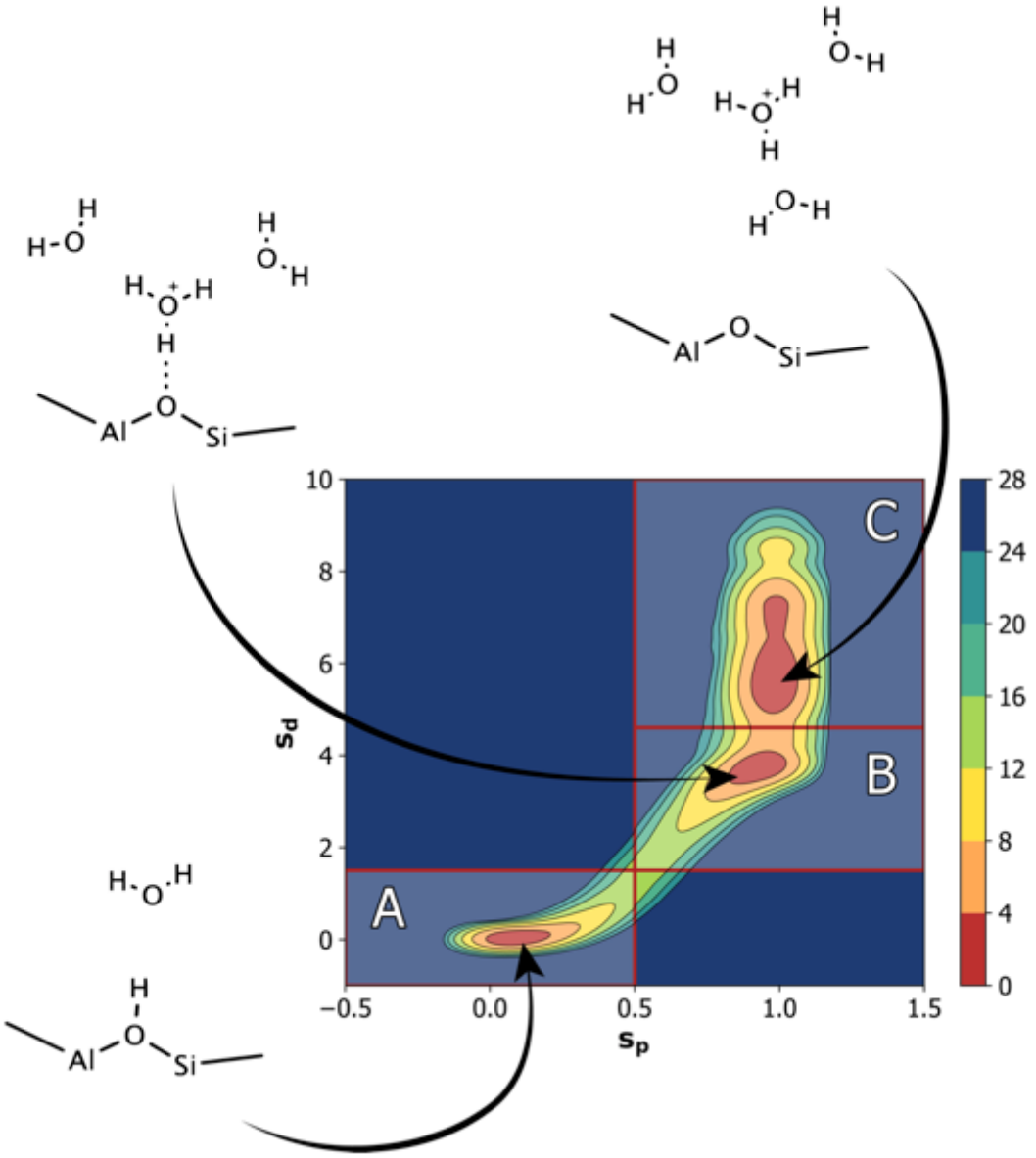

Figure 6

The three thermodynamic states visible in the free energy surface and the relative structures.

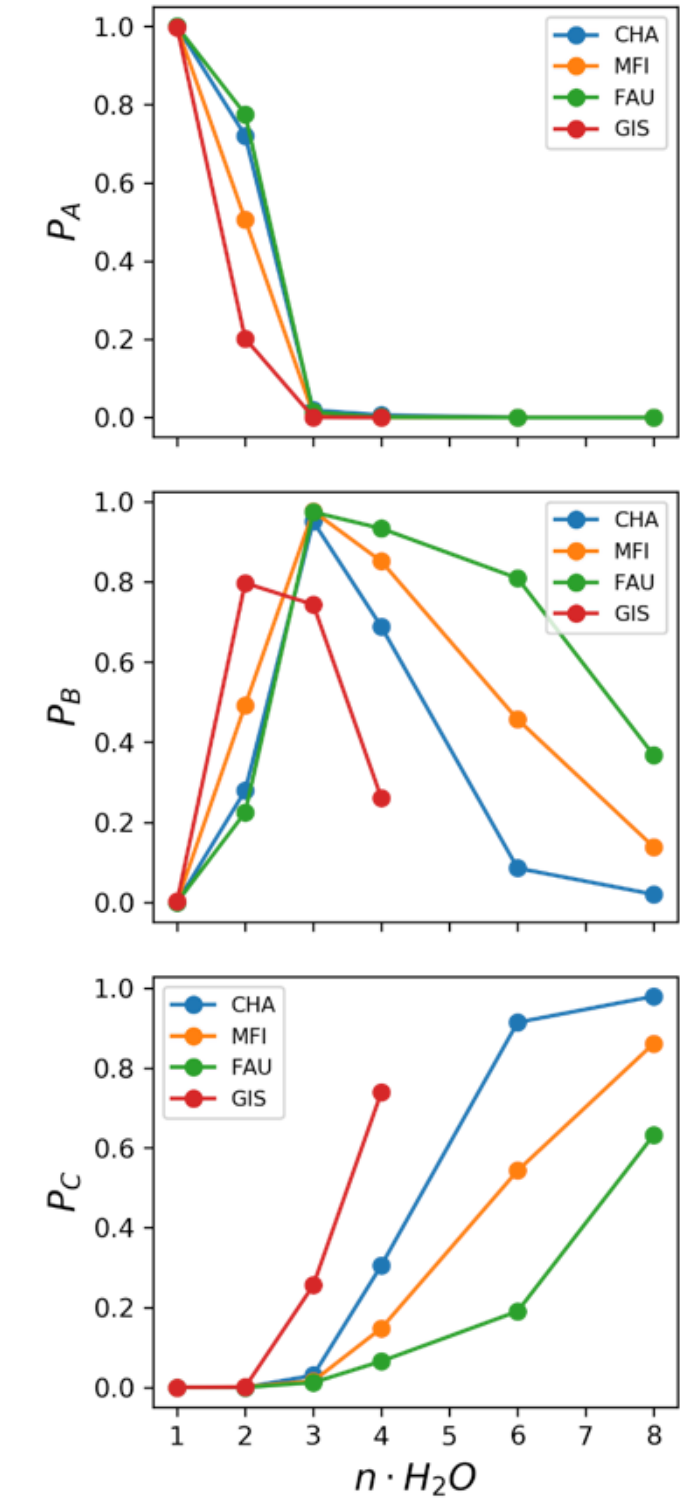

Figure 7

Relative population in each thermodynamic state for every zeolite at different level of water loading.

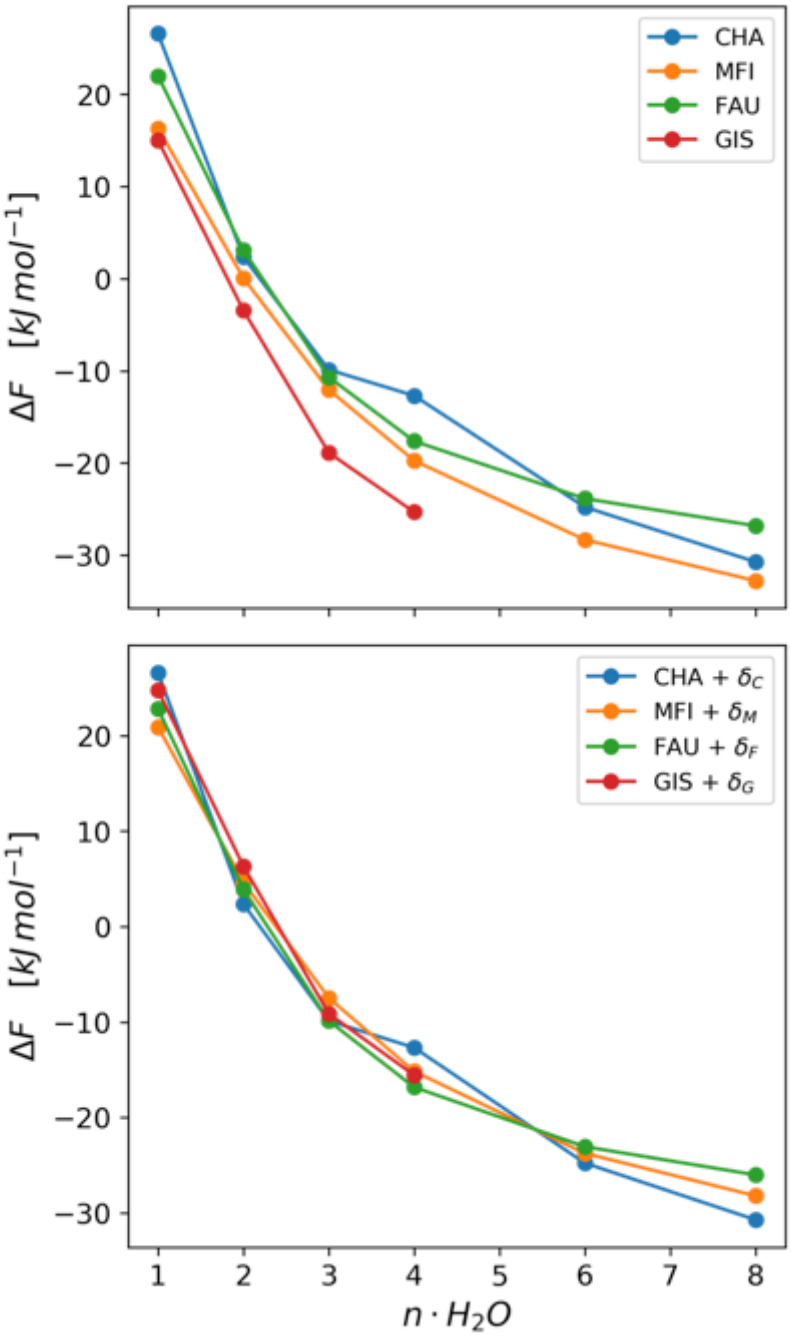

Figure 8

Differences in free energy between states A and B+C as a function of the water loading (top panel) and same curves rescaled by a factor δ that minimize the offsets among them. δc = 0, δm = 4.56, δF = 0.79, δG = 9.75.

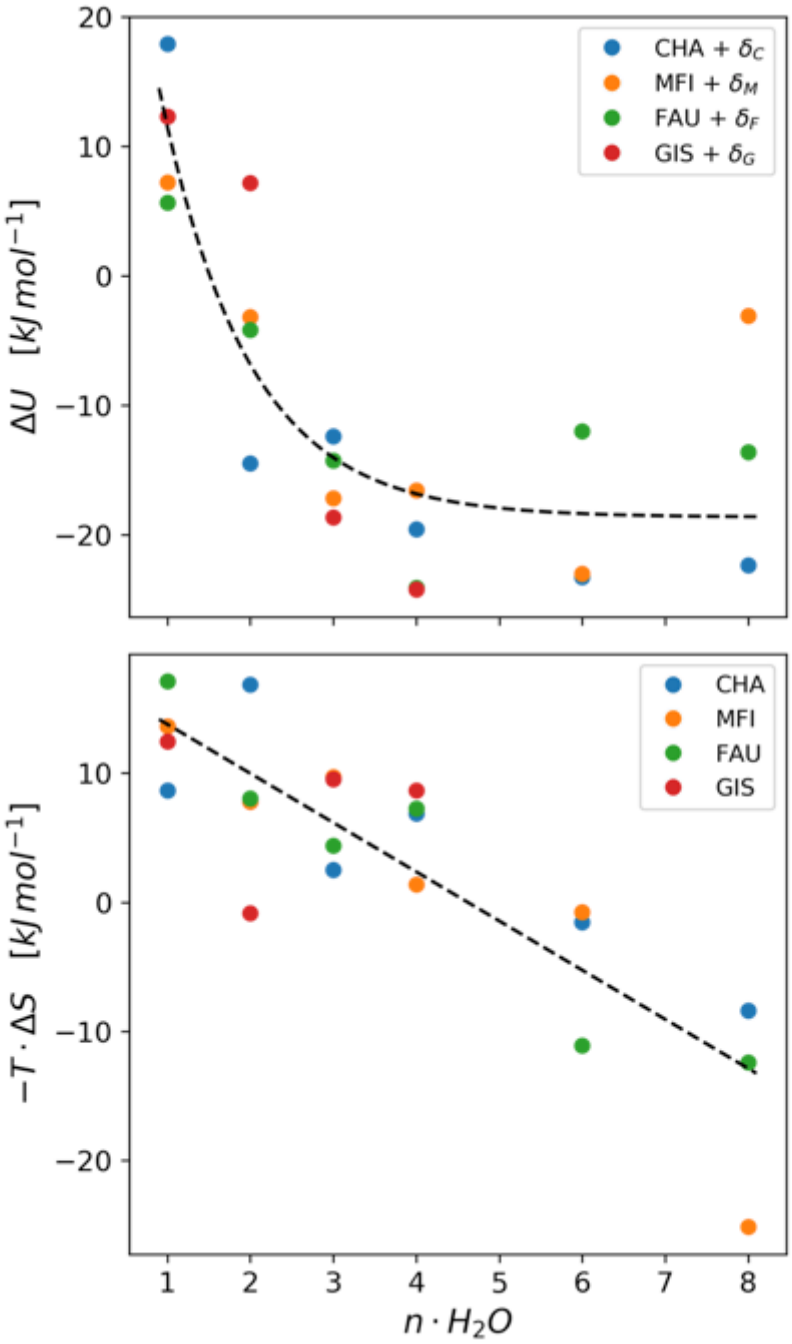

Figure 9

Exponential and linear decay of the enthalpic and entropic contribution to the generation of the hydrated hydronium ion.

Supplementary Files

This is a list of supplementary files associated with this preprint. Click to download.

- SI.docx